Numerical computation of tunneling fluxes

Michael Galperin
School of Chemistry, Tel Aviv University, Tel Aviv 69978, Israel

Sivan Toledo
School of Computer Science, Tel Aviv University, Tel Aviv, 69978, Israel

Abraham Nitzan
School of Chemistry, Tel Aviv University, Tel Aviv 69978, Israel

The computation of tunneling probabilities in three dimensions is a numerical challenge, because the small transition probabilities associated with the overlap of exponentially vanishing wave function-tails require large computational accuracy. In scattering situations arising, e.g., in electron tunneling in metal-molecule-metal junctions, this is compounded by the need to provide a proper truncation procedure at the numerical boundaries of the computed system and by the need to account for electrostatic fields and image interactions. This paper describes a numerical methodology to deal with these problems. A pseudopotential that describes the underlying system is assumed given. Electrostatic fields and image interactions are evaluated for the given boundary conditions from numerically solving Laplace and Poisson equations. Tunneling probabilities are computed using a grid-based absorbing boundary conditions Green's function method. An efficient and exact way to implement the absorbing boundary conditions by using the exact self-energy associated with separating the scattering system from the rest of the infinite space is described. This makes it possible to substantially reduce the size of the grid used in such calculations. Two applications, an examination of the possibility to resolve the spatial structure of an electron wave function in an electron cavity by scanning tunneling microscopy, and a calculation of electron tunneling probabilities through water, are presented. © *2002 American Institute of Physics.*
[DOI: 10.1063/1.1522404]

I. INTRODUCTION

Tunneling phenomena are pervasive in many processes that involve low temperature transport of light particles, and in the context of atomic and molecular processes are most frequently encountered in electron and proton transfer reactions. While simple analytical solvable one-dimensional models are often used as guides for understanding observations of tunneling transport, detailed three-dimensional calculations are needed for full analysis. As a case in point consider electron transfer in condensed molecular environments such as water or proteins. Following Marcus,[1,2] early treatments of such processes have used continuum dielectric pictures to treat solvent effect on electron transfer. This approach has been quite successful in elucidating the qualitative phenomenology of electron transfer processes that are dominated by solvent induced fluctuations in the donor and acceptor energy levels, by describing these fluctuations using the macroscopic solvent polarization through the frequency dependent dielectric response. However, a quantitative determination of the transfer rate requires the evaluation of the tunneling matrix element, i.e., the electronic coupling between the donor and acceptor. This coupling depends strongly on the structure of the molecular medium separating between the donor and acceptor sites, and its evaluation amounts to evaluating the tunneling rate between these sites separated by a three-dimensional potential barrier of relatively complex nuclear and electronic structure. Considerable amount of work has been done during the past two decades using quantum chemical electronic structure calculations to evaluate such electronic coupling elements for intramolecular electron transfer processes and for electron transfer between donor and acceptor species in protein environments.

The need to determine such three-dimensional tunneling matrix elements is particularly important in analyzing processes that involve electron transmission through molecules or molecular layers that separate between regions of free or quasi-free electrons, e.g., metal electrodes.[3] Such processes are encountered in metal-molecule-metal junctions and recent interest in their study stems from the need to understand the ''underwater'' (i.e., in solution) operation of the tunneling electron microscope on the one hand, and from recent studies of molecular junctions where a molecule or a molecular aggregate is used as a conductor connecting two metal leads, on the other. The transferred electron (or more generally, the charge carrier) in such systems is not localized in the initial and final states, therefore the transfer process is not dominated by solvent reorganization, leaving the tunneling matrix elements as the main factor that determines the transmission rate or the tunneling current.

Depending on the spacer between the two metal leads, calculation of electron transmission (e.g., current–voltage characteristics) in such systems can be carried out using an appropriate basis set of molecular or atomic orbitals. Alternatively, in deep tunneling regimes, where the electron en-
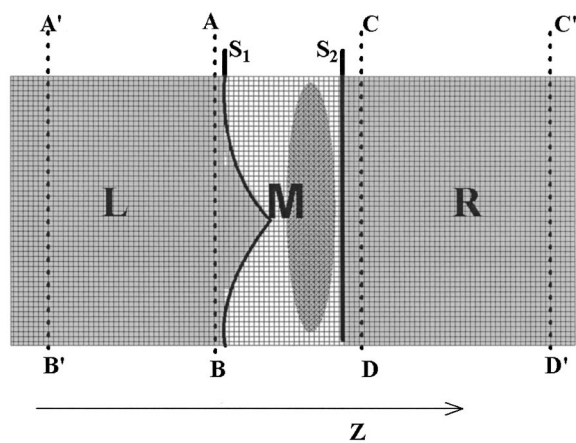
10818   J. Chem. Phys., Vol. 117, No. 23, 15 December 2002

Galperin, Toledo, and Nitzan

FIG. 1. A model system used to compute electron transmission between two electrodes, L and R separated by a narrow spatial gap (M) containing a molecular species. The surface S_1 of L is shaped to mimic a tip. The lines $A'B'$, $C'D'$ and AB and CD are projections of boundary surfaces normal to the transmission direction (see text for details). The numerical solution is carried on a grid (shown).

ergy is far from resonance with any molecular level and tunneling takes place mostly or partly in intermolecular space, a spatial grid basis may be used if a suitable pseudo-potential for the electron-molecule interaction is available. In several recent papers we have used such an approach to investigate electron tunneling through water. The present paper discusses several methodological issues involved in such a calculation. We discuss two generic issues that should be considered in all calculations of this type. These are (a) the handling of the electrostatic interactions (electric field distribution and image effects) and (b) the use of absorbing potentials. Together with the (assumed given) electron-molecule pseudopotential and the bare potential associated with the electrode-vacuum interface (most simply modeled as a potential step with height derived from the metal work-function), the representation of the Hamiltonian on a suitable grid and an adequate numerical method to evaluate needed Green's function matrix elements, the end result provides a framework for computing single electron tunneling probabilities in metal-molecule-metal junctions under bias.

Figure 1 illustrates the nature of our problem. It represents a two-dimensional cut through a three-dimensional junction made of two metal electrodes (the bulk gray areas whose edges in the junction region are the black lines denoted S_1 and S_2) and a molecular entity (represented by the dark-shaded ellipsoid). A potential bias is employed between the electrodes and the resulting current is monitored. The fact that the electrode surfaces are generally nonplanar is represented in the figure by the tiplike shape of the left electrode. In the absence of thermal interaction the linear conductance of this junction is given by the multichannel Landauer formula

$$g(E) = \frac{e^2}{\pi\hbar} \mathcal{T}(E_F) \qquad (1)$$

that connects the conduction g to the multichannel transmission probability $\mathcal{T}(E)$

$$\mathcal{T}(E_F) = \sum_{i,f} \mathcal{T}_{if}(E_F). \qquad (2)$$

Here $\mathcal{T}_{if}$ is the transition probability from the incoming state i to the outgoing state f, the sum over i and f is over all states ("channels") associated with the electron on the left and right electrodes, respectively, and E_F is the Fermi energy. In another context, the reactive flux theory of Miller and co-workers $\mathcal{T}(E)$ has been termed the "all to all" transition probability. The important point is that in this dissipationless single electron theory, the conduction of a given junction is related to $\mathcal{T}$, a result from scattering theory. Indeed, evaluating $\mathcal{T}$ amounts to solving a three-dimensional single particle potential scattering problem in a rather complex scattering potential, where for a particle incident on the target (i.e., the junction) from the left electrode the "reactive flux" is the flux traveling in the right electrode in the positive z direction.

As already stated, in energy ranges where this quantum scattering problem can be expressed using a given molecular basis set in the junction, standard quantum chemistry methods can be employed to evaluate $\mathcal{T}$. Alternatively, if the electron-target interaction is reliably modeled by a local potential it is convenient to use a basis based on a spatial grid. We have found that a cubic grid (whose two-dimensional projection is shown in Fig. 1) on which the kinetic energy operator is represented by a standard differencing approximation[4] can yield a reasonably accurate transmission probability, provided the mesh size is chosen to give a reliable representation of the scattering potential. In a typical calculation periodic boundary conditions are employed in the x and y directions parallel to the electrode surfaces, while in the tunneling direction z the calculation is restricted to a finite segment M, say between surfaces AB and CD in Fig. 1, of the infinite system by projecting out the rest of the electrode bulks. This gives rise to self-energy terms in the Green's function associated with M. The all-to-all transition probability is given by[5]

$$\mathcal{T}(E) = \text{Tr}[G(E)\Gamma_R(E)G^\dagger(E)\Gamma_L(E)], \qquad (3)$$

where $G(E)$ is the retarded Green's function of M, i.e., with $(H_M)_{ij} = H_{ij}$ where i and j are grid points in the segment M

$$G(E) = [E - H_M - \Sigma(E)]^{-1}. \qquad (4)$$

$\Sigma(E)$ is the retarded self-energy resulting from projecting out the rest of the electrode bulks and $\Gamma(E) = \Gamma_L(E) + \Gamma_R(E)$ is twice its negative imaginary part with contributions $\Gamma_L(E)$ and $\Gamma_R(E)$ associated with the left and right electrodes. The Tr operation corresponds to a sum over all diagonal terms, $\text{Tr} = \Sigma_i(\ )_{ii}$. It should be emphasized that the calculation of $\mathcal{T}(E)$ should be done under the given potential bias $\Delta\Phi$ between the two leads. The tunneling current for this voltage is then computed from Ref. 6:

$$I = \frac{e}{\pi\hbar} \int_0^\infty dE[f_L(E) - f_R(E)]\mathcal{T}(E). \qquad (5)$$

To evaluate the transmission probability (3) we need (a) to get an expression for the self-energy matrices Σ and Γ, and (b), to invert the matrix in Eq. (4). In much of the computational scattering theory literature the calculation of the

self-energy is circumvented by using the observation that, if the mathematical boundaries of the segment S on which the calculation is made are set far enough from the target (e.g., in Fig. 1 replace the boundaries AB and CD by $A'B'$ and $C'D'$, respectively), the resulting self energy should simply reflect the fact that a particle crossing these boundaries in the outward direction is not reflected back and therefore disappears forever from the system. One then sets $\text{Re}\,\Sigma(E)=0$ and replaces $\Gamma_L(E)$ and $\Gamma_R(E)$ by simple energy independent absorbing potentials $\Gamma_L(E)\to 2\epsilon_L(z)$ and $\Gamma_R(E)\to 2\epsilon_R(z)$ that are chosen to affect this reflectionless propagation through the left and right boundaries of the system S. In this absorbing boundary conditions Green's function ($ABCGF$) formalism Eq. (3) becomes

$$\mathcal{T}(E)=4\,\text{Tr}[G(E)\epsilon_R G^\dagger(E)\epsilon_L]. \tag{6}$$

For example, in our previous calculations we have employed the form

$$\epsilon_{L,R}(z)=\left(\frac{2|z|}{L_z}\right)^7 \tag{7}$$

that expresses the need for a very smooth rise of these absorbing potentials toward the boundaries needed to avoid reflection. Noting that in tunneling calculations we often encounter the need to compute transmission coefficients of order, say, 10^{-10}, the necessity to avoid even the small reflection that will cause an error of this magnitude makes it necessary to use a very gradual rise of $\epsilon(z)$, as seen in Eq. (7), which in turn makes it necessary to increase the system size in the z direction. Typically, the system size in this direction was taken 3–4 times larger than the actual size of the target (expressed by the range of the electron-target potential) in implementations of Eq. (6), and a typical spatial grid used[7–13] in calculations of electron tunneling through a water layer made of, say, three monolayers (thickness ~ 10 Å) was $16\times16\times400$ with lattice spacing of the order of 0.1 and 1.46 Å in the tunneling and in the lateral directions, respectively. This implies the need to invert matrices of order $\sim 10^5$ to get $G(E)$, and a sum over a number of points of the same order to calculate the trace in Eq. (6). For this reason our earlier calculations were restricted to the one-to-all transmission probability associated with a particular incoming state l on the left (say) that in the $ABCGF$ formalism is given by

$$P_l(E)=\frac{2}{\hbar}\langle l|\epsilon_L G^\dagger(E)\epsilon_R G(E)\epsilon_L|l\rangle. \tag{8}$$

Obviously, if exact expressions for the self-energy were available one could use Eq. (3) with the boundaries AB and CD placed right on the edge of the target. In practical calculations we have found that implementing this idea makes it possible to reduce substantially the size of the calculational system in the z direction, providing saving of at least an order of magnitude in both the memory requirement and the CPU time needed.

Another important, and not completely solved problem is the need to evaluate the electrostatic and polarization interactions that affect the tunneling electron. Two issues are involved. First, for a given potential bias the electrostatic field distribution between the electrodes is needed. Second,

the polarization response of the metal electrodes to the excess electron in the junction, what is sometimes called the image effect is potentially an important ingredient in this calculation. If we take the electrode surfaces as classical electrostatic boundaries the first issue is conceptually straightforward, and the external field distribution in the junction may be obtained from solving the Laplace equation with the Dirichlet boundary conditions on the electrode surfaces. The second issue is highly nontrivial, since using simple static image to account for metal electronic response to the excess electron in the junction is just a poor man's approach to a very complex many electron problem. A similar problem arises when the response associated with the molecular electronic polarizability in the barrier to the tunneling electron is considered. If the time scale for this response is fast relative to the timescale of the tunneling event, a simple local potential associated with this polarizability response can be constructed. We have argued[13] that such an approach provides a reasonable approximation for electron tunneling through water. Similarly, if the timescale associated with a tunneling event is slow relative to the metal response time, static image should provide a reasonable approximation for the metal response. The metal response time can be estimated from the plasma frequency, of order $10^{16}\,\text{s}^{-1}$, while the relevant for a tunneling event through a barrier of height 1 eV and width 10 Å is estimated to be $\sim 10^{15}\,\text{s}^{-1}$. This justifies the use of static image in such tunneling calculations and we will adopt this approach here as has been done many times in the past following Ref. 14. Evaluating the static image between electrodes of arbitrary shape constitutes a nontrivial numerical problem that we discuss below.

A numerical calculation of electron tunneling in a biased junction within the framework described above thus requires: (a) evaluating the electrostatic field distribution in the barrier; (b) evaluating the image interaction as a local potential affecting the electron; (c) having a suitable pseudopotential that describes the interaction of the tunneling electron with the underlying molecular system; (d) deriving and testing suitable absorbing potentials that allow to truncate the system in the tunneling direction, or alternatively evaluating the exact self-energy associated with this truncation; (e) Setting the scattering Hamiltonian on a spatial grid and using a suitable numerical inversion algorithm to evaluate the needed Green's function matrix elements.

Common to steps (a), (b), and (e) is the need to invert large sparse matrices. Krylov space based iterative methods[15] are particularly suitable for this task. In our applications we have used the implementation of this method provided in the PETSc package.[16]

Some of these issues have been described in our recent publications. This paper deals with recent developments in the methodology used for others. The next section provides the details of our numerical approach to the electrostatic part of our problem. In Sec. III we describe the way the absorbing boundary conditions are constructed. Two applications, an examination of the possibility to resolve the spatial structure of an electron wave function in an electron cavity and a

10820   J. Chem. Phys., Vol. 117, No. 23, 15 December 2002

Galperin, Toledo, and Nitzan

calculation of electron tunneling probabilities through water, are presented in Sec. IV. Section V concludes.

II. ELECTROSTATIC AND IMAGE INTERACTIONS

Between the two metal surfaces the tunneling electron moves in an external field imposed by the potential drop. The distribution of this field between the electrodes is obtained from the Laplace equation

$$\nabla^2 \Phi = 0 \tag{9}$$

using a finite differencing scheme on the given lattice, e.g.,

$$\frac{\partial^2}{\partial x^2} \Phi(i,j,k) = \frac{\Phi(i+1,j,k) - 2\Phi(i,j,k) + \Phi(i-1,j,k)}{h_x^2}, \tag{10}$$

where (i,j,k) is a grid point and h_x is the grid spacing in the x direction. Periodic boundary conditions in the x and y directions are naturally contained within this scheme, and the Dirichlet (potential) boundary conditions on the surfaces S_1 and S_2 appear as fixed terms in the l.h.s. of Eq. (9). Taking these terms to the r.h.s., Eq. (9) takes the form

$$\mathbf{A}\Phi = \mathbf{b}, \tag{11}$$

where the potential Φ is now represented by a vector of the order of the total number of grid points n. The boundary-conditions vector $\mathbf{b}$ is of the same order, while $\mathbf{A}$ is an $n \times n$ matrix. In the more general case of position dependent dielectric response characterized by a dielectric function $\epsilon(\mathbf{r})$ Eq. (9) becomes

$$\nabla \cdot [\epsilon(\mathbf{r}) \nabla \Phi(\mathbf{r})] = 0. \tag{12}$$

Particular care must be exercised in cases where the inhomogeneous medium is described by a discontinuous dielectric function, e.g., in a model system with different dielectric media separated by distinct boundaries. In this case the discretization scheme (10) becomes[17,18]

$$\nabla \cdot [\epsilon(\mathbf{r}) \nabla \Phi(\mathbf{r})] \rightarrow \frac{C_{i,j,k}^{i+1,j,k}[\Phi(i+1,j,k) - \Phi(i,j,k)] - C_{i-1,j,k}^{i,j,k}[\Phi(i,j,k) - \Phi(i-1,j,k)]}{h_x^2}$$

$$+ \frac{C_{i,j,k}^{i,j+1,k}[\Phi(i,j+1,k) - \Phi(i,j,k)] - C_{i,j-1,k}^{i,j,k}[\Phi(i,j,k) - \Phi(i,j-1,k)]}{h_y^2}$$

$$+ \frac{C_{i,j,k}^{i,j,k+1}[\Phi(i,j,k+1) - \Phi(i,j,k)] - C_{i,j,k-1}^{i,j,k}[\Phi(i,j,k) - \Phi(i,j,k-1)]}{h_z^2}, \tag{13}$$

where

$$C_{l,m,n}^{i,j,k} = 2\frac{\epsilon(i,j,k)\epsilon(l,m,n)}{\epsilon(i,j,k) + \epsilon(l,m,n)}. \tag{14}$$

Consider now the evaluation of the image potential of a point charge positioned in the space between the two metal electrodes in a tip-substrate geometry such as shown in Fig. 1. This image potential arises from the polarization induced on the electrodes by the point charge. The total potential associated with a given charge distribution $\rho(\mathbf{r})$ in an inhomogeneous dielectric environment can be computed from the Poisson equation equivalent of Eq. (12)

$$\nabla[\epsilon(\mathbf{r})\nabla\Phi(\mathbf{r})] = -4\pi\rho. \tag{15}$$

On a grid this leads again to Eq. (11), with a $\mathbf{b}$ vector that is modified to take into account the existence of the charge distribution ρ. For example, for a point charge q located on the grid point ℓ we have $b_n \rightarrow b_n - [4\pi q/h_x h_y h_z]\delta_{nl}$. To evaluate the image potential of such a point charge we need to subtract from Φ its singular part that will amount to an interaction of the charge with itself.[19] In addition we need to correct for the unphysical effect of the periodic boundary conditions taken in the lateral $\mathbf{r}_\parallel = x, y$ directions, that would result in false contributions to Φ from the periodic replicas of both ρ and its images. An approximate correction scheme is as follows. We solve Eq. (15) once for $\Phi_1(\mathbf{r}_\parallel, z)$—the

potential of a point charge in the desired tip-plane geometry and once for $\Phi_2(z)$—the potential of a point charge at the same position between two parallel planar electrodes. In the difference $\Delta\Phi(\mathbf{r}_\parallel, z) = \Phi_1(\mathbf{r}_\parallel, z) - \Phi_2(z)$ the self-energy singular part is eliminated. Also much of the unphysical contribution of the periodic replicas is eliminated. (The interaction of the electron with its own replicas is eliminated but not its interaction with the replicas of the tip, which still leaves a small error in the resulting potential.) $\Delta\Phi$ is therefore an approximation to the difference between the image potential of a point charge in the space between the tipped and the flat electrodes and the potential of a similar point charge between two planar electrodes. An analytical expression for the latter is known[20]

$$\Phi_I^{\text{flat}}(z_0) = \sum_{k=1}^{\infty} \left(\frac{1}{L_z k} - \frac{1}{L_z(2k-1) - 2z_0} \right.$$

$$\left. - \frac{1}{L_z(2k-1) + 2z_0} \right), \tag{16}$$

where L_z is the distance between the two electrode surface planes and z_0 is the position of the point charge measured from the mid-point between these planes. Our final approximate expression for Φ_I is thus

$$\Phi_I(\mathbf{r}_\parallel, z_0) = \Delta\Phi(\mathbf{r}_\parallel, z_0) + \Phi_I^{\text{flat}}(z_0). \tag{17}$$

J. Chem. Phys., Vol. 117, No. 23, 15 December 2002

Numerical computation of tunneling fluxes   10821

To summarize, the numerical calculation of the image potential of a point charge positioned between a tipped and a flat surfaces is obtained by solving the Poisson equation (15) twice, once for our actual geometry and once for the equivalent system without the tip, i.e., a point charge between two flat electrodes, and forming the difference $\Delta\Phi$ between these solutions. Φ_I is then obtained from Eqs. (16) and (17).

III. ABSORBING BOUNDARY CONDITIONS

As noted in the Introduction, the absorbing boundary conditions Green's function method in computational scattering theory is essentially just a way to circumvent the need to evaluate exact self-energy terms that arise when an infinite space process is described within the framework of a finite subspace. In our application (Fig. 1) the outcome of the scattering process is determined by interactions that vanish beyond the target region, which is confined between the planes represented by the projections AB and CD. Also here, the physics of the process is defined by the fact that outgoing waves are never reflected back into the interaction region. Adding absorbing potentials that vanish in the target region and rise smoothly as $|z| \to \infty$ achieves this goal at the cost of having to deal with much bigger systems, say between the planes $A'B'$ and $C'D'$. Alternatively, we could limit the size of our computational grid to the system confined between planes AB and CD if we use Eqs. (3) and (4) with the correct self-energies. This is often done in computations involving tight-binding models in solid-state physics, where the inherent lattice symmetry makes it possible to find a closed set of equations for the required self-energy and several methods have been developed for this purpose.[21–27] In the present paper we consider single electron transmission problems in which the Hamiltonian of the system is defined on a spatial grid. In this representation the potential is a local operator that vanishes outside the molecular "target," while the kinetic energy has a tight binding form.[4] Therefore the same methods for evaluating the exact self-energy are applicable as detailed below. Note that the absorbing potential derived in this way is naturally energy dependent. A different approach that yields an exact energy independent complex absorption potential was recently derived by Moiseyev.[28,29]

In general, the Hamiltonian for our problem (see Fig. 1) has the form

$$\mathbf{H} = \begin{pmatrix} \mathbf{H}_L & \mathbf{H}_{LM} & 0 \\ \mathbf{H}_{ML} & \mathbf{H}_M & \mathbf{H}_{MR} \\ 0 & \mathbf{H}_{RM} & \mathbf{H}_R \end{pmatrix} \tag{18}$$

and the M-space retarded Green's operator is

$$\mathbf{G}_M(E) = [E - \mathbf{H}_M - \mathbf{\Sigma}_L(E) - \mathbf{\Sigma}_R(E)]^{-1}, \tag{19}$$

$$\mathbf{\Sigma}_K(E) = \mathbf{H}_{MK}(E - \mathbf{H}_K + i\epsilon)^{-1}\mathbf{H}_{KM}; \quad K = L, M. \tag{20}$$

A self-consistent procedure for evaluating $\mathbf{\Sigma}_R$ (and similarly $\mathbf{\Sigma}_L$) is obtained by exploiting the fact that the Hamiltonian matrix is nearly diagonal. If the division between M and R is set deep enough in the electrode region so that H_{MR} connects only sites on the electrode's surface, the nonzero elements of $\mathbf{\Sigma}_R$ may be obtained from the following consideration concerning the surface Green's function of R. Let S denotes the surface of R, i.e., all lattice sites on the n_S leftmost planes of R (n_S is chosen to be equal or larger than the range of the nondiagonality of R, determined from the way the kinetic energy matrix is set. H_R, a semi-infinite nearly diagonal matrix has the form[30]

$$\mathbf{H}_R = \begin{pmatrix} \mathbf{H}_R^s & \mathbf{H}_{SR} \\ \mathbf{H}_{RS} & \mathbf{H}_R \end{pmatrix}. \tag{21}$$

This form reflects the fact that the sub-system remaining after the surface layer is removed from the semi-infinite reservoir is identical to the original reservoir. The surface Green's function, the projection $\mathbf{G}_R^s(E) = [(E - \mathbf{H}_R + i\epsilon)^{-1}]_{SS}$ of $\mathbf{G}_R(E)$ onto the S-subspace is also given by

$$\mathbf{G}_R^s(E) = [E - \mathbf{H}_R^s - \mathbf{\Sigma}_R^s(E)]^{-1}, \tag{22}$$

where

$$\mathbf{\Sigma}_R^s(E) = \mathbf{H}_{SR}(E - \mathbf{H}_R + i\epsilon)^{-1}\mathbf{H}_{RS}. \tag{23}$$

Here we use the fact that the space obtained by removing the surface S from R is identical to R. Since the coupling $\mathbf{H}_{SR}$ involves only the surface (n_S planes) of the "new" R space we have

$$\mathbf{\Sigma}_R^s(E) = \mathbf{H}_{SR}[E - \mathbf{H}_R^s - \mathbf{\Sigma}_R^{s(E)}]^{-1}\mathbf{H}_{RS}. \tag{24}$$

This constitutes a self consistent equation for the surface self-energy $\mathbf{\Sigma}_R^s(E)$ that may be solved iteratively. Actual implementations of this idea use different methods (resolvent matrix approach,[21] a recursive scheme,[22,23,31] renormalization group or decimation technique,[24–26] and a matrix-valued extension of the Möbius transformation method[27]) to enhance convergence. In our calculation we have used an adaptation of the decimation technique of Refs. 25, 26, outlined in Appendix A.

Once a converged matrix $\mathbf{\Sigma}_R^s$ is obtained from this calculation it can be identified with the self-energy $\mathbf{\Sigma}_R$ needed in Eq. (19). A similar procedure yields $\mathbf{\Sigma}_L$. In particular, if we use the simplest 3 point approximation for the kinetic energy operator, for which the kinetic energy matrix is tridiagonal, then $n_S = 1$ and in $\mathbf{k}_\parallel$ space ($\parallel$ is the direction parallel to the electrode surfaces) Eq. (24) becomes a set of independent equations for $\mathbf{\Sigma}_R^s(\mathbf{k}_\parallel, E)$. In our usual application of a 7-point approximation for the kinetic energy $\mathbf{\Sigma}_R^s(\mathbf{k}_\parallel, E)$ is a 3×3 matrix.

Obviously the all-to-all transmission flux may be obtained also by summing the $ABCGF$ one-to-all transmission probability, Eq. (8), over all initial states l of energy E. If $|l\rangle = (v_l)^{-1/2}\exp(i\mathbf{k}_l \cdot \mathbf{r})$ is defined on the left of the barrier, this implies summing over all directions of the incident wave-vector $\mathbf{k}_l(v_l = \hbar|k_l|/m)$. Note that because we usually apply periodic boundary conditions in the lateral directions, only a finite discrete number of such wave vectors are relevant. This has provided a useful check on the applicability of the exact self-energy—based calculation using Eq. (6) (see Fig. 6 below).

To end this section we note that a spatial grid representation corresponds to describing the system in terms of a particular orthonormal basis in which the potential energy operator is diagonal. In many practical situations it is conve-

nient to describe a molecular bridge using the nonorthogonal basis of atomic wave functions. The Hamiltonian still takes the form (18) but Eqs. (19) and (20) are replaced by $\mathbf{G}_M(E) = [\mathbf{h}_M - \mathbf{\Sigma}_L(E) - \mathbf{\Sigma}_R(E)]^{-1}$ where $\mathbf{h} = E\mathbf{S} - \mathbf{H}$ and $S_{ij} = \langle \phi_i | \phi_j \rangle$. A commonly used approximation for the self-energy in this case is $\mathbf{\Sigma}_K(E) = \mathbf{h}_{MK}(E\mathbf{S} - \mathbf{H}_K + i\epsilon)^{-1}\mathbf{h}_{KM}$; $K = L, M$. A procedure for its calculation is given in Appendix B.

IV. APPLICATIONS

In the examples discussed below we consider electron tunneling through a spacer separating two biased electrodes. The potential H_M in Eq. (18) is then a superposition of the pseudopotential describing the interaction between the electron and this "target" and the electrostatic potential associated with the given potential boundary conditions, calculated from solving the corresponding Poisson and Laplace equations as described in Sec. II.

A. Imaging the structure of a cavity-confined wave function

We first apply the methodology discussed above to a simple three-dimensional scattering calculation aimed at assessing the possibility to resolve the structure of cavity-confined wave functions in a standard STM measurement. Such an experiment was recently reported by Dekker and co-workers[32] where the cavity is provided by a short carbon nanotube deposited on a gold substrate, and it was observed that the conduction in the direction normal to the tube axis as a function of the tip displacement along this axis can, for some potential bias conditions, reflect the standing wave character of the electronic wave function confined in the tube rather than the underlying atomic structure. In the calculation described below we mimic the nanotube by a long rectangular cavity in an otherwise square barrier (see Fig. 2). An energy diagram showing the positions of the lowest energy levels of the cavity relative to the Fermi and the vacuum energies is shown in Fig. 3.

Evaluation of the tunneling current according to Eqs. (3) and (5) is done on a rectangular grid with $25 \times 13 \times 79$ points and lattice spacings $2 \times 2 \times 0.2$ Å. Periodic boundary conditions are used in the x and y directions, while absorbing boundary conditions are set on the boundary planes normal to the z axis using the procedure described in Sec. III. The potential experienced by the tunneling electron is taken to be a superposition of the bare potentials in the electrodes, cavity and vacuum regions (see caption to Fig. 2), with the electrostatic potential arising from the voltage bias and with the image potential associated with the response of the metal boundaries to the moving electron. As discussed in Sec. I, the latter is assumed to be instantaneous. In addition, an artificial high barrier is added on the flat part of the upper electrode surface, restricting transmission to the tip region (this mimics the real-life situation in which the tip is much longer than in our numerical model). In our calculation the potential at the substrate is kept zero, that of the tip and the upper electrode is varied, and the electrostatic potential distribution in the system between the electrodes is obtained from the solution of the corresponding Laplace equation (see Sec. II). Simi-
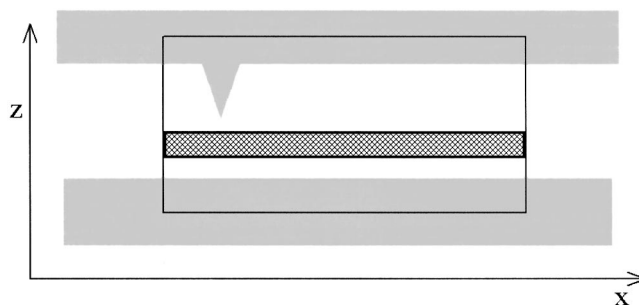

FIG. 2. A side view of the model used to demonstrate STM resolution of confined wave function. The distance between the two planar electrodes is 16 Å. The tip is a cone protruding from the upper electrode, of height 6 Å and opening angle 30°. In the absence of bias, the potentials in the gray areas that represent the electrodes and in the white region (vacuum) are taken 0 and 5 eV, respectively. The work functions of the two electrodes are taken to be 3 eV (Ref. 33). The rectangular crossed area represent the cavity, whose dimensions are taken $30 \times 5 \times 5$ Å. The potential in this cavity is set to be 1 eV, i.e., in the vacuum it forms a rectangular potential box of depth 4 eV. These potentials are superimposed with the potential distribution associated with the voltage drop between the electrodes and with the image potential, both computed as described in the text. The distances between the tip edge and the cavity, and between the cavity and the substrate are 3 and 2 Å, respectively. The tip is set above the center of the cavity in the direction y perpendicular to the paper, and the current is computed as a function of its position along the x direction for different potential biases. The region surrounded by the thin-lined rectangle is the projection of the system used in the calculation on the plane of the figure. The cavity is situated in the center of this region in the x and y directions.

larly, the image potential was obtained from the solution of a Poisson equation using the procedure described in Sec. II. In both electrostatic calculations we have used the same rectangular grid used in the quantum calculation.

Some results of these calculations are shown in Fig. 4. The different lines depict the computed current plotted against the tip displacement in the x direction. It is seen that the spatial structure of the wave functions is reflected in the spatial modulation of the tunneling current. Clearly, with the exception of the lowest state observed at low bias voltages,
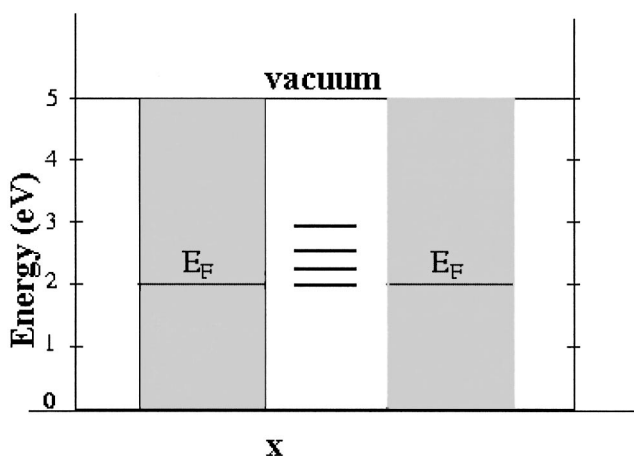

FIG. 3. The energetics of the transmission problem of Fig. 2 in the absence of a bias potential. The gray areas represent the substrate and tip electrodes with their common Fermi energy E_F. The energy levels depicted in the center are the lowest eigenstates of the cavity (computed on our grid using a Lanczos algorithm). The levels shown are all nodeless in the y and z directions, i.e., correspond to increasingly shorter wavelengths in the x direction.
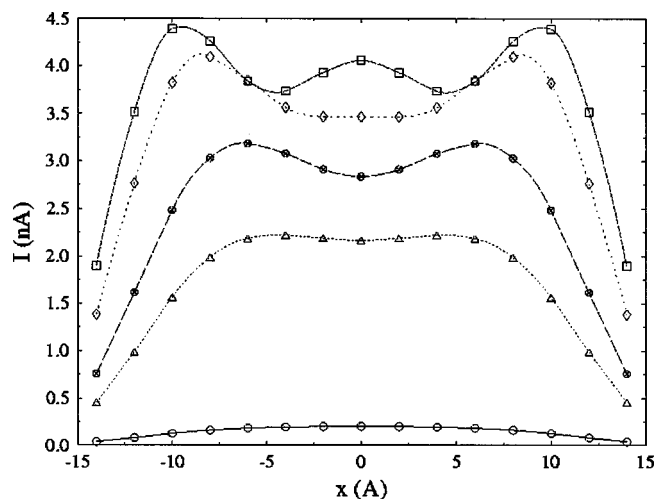
FIG. 4. The current calculated at $T = 300$ K in the system of Fig. 2 (with Fermi energy $E_F = 2$ eV for both tip and substrate[33]) displayed as a function of the tip position along the x direction ($x = 0$ is the center of the cavity). The different lines correspond to different tip potentials (the substrate potential is taken zero): $\bigcirc$-$\Phi = 100$ mV, $\triangle$-$\Phi = 326$ mV, $\otimes$-416 mV, $\diamond$-568 mV, $\square$-742 mV.

more than one cavity state contribute to the tunneling current at higher voltages and the spatial modulation seen in Fig. 4 reflects combination of several wavefunctions. As noted in Ref. 32, the spatial modulation of the conduction, $dI/d\Phi$, can be dominated by a single barrier state if Φ is chosen so that the transmission dominated by the corresponding resonance. Figure 5 demonstrate this point by displaying together the average conduction in the 568–742 mV range, $\bar{G} = [I(\Phi = 742 \, \text{mV}) - I(\Phi = 568 \, \text{mV})]/174$, which is dominated by the resonance associated with the second excited cavity state and the probability density associated with this state.[33,34] Obviously, $\bar{G}$ reflects the distribution of this density much better than I.
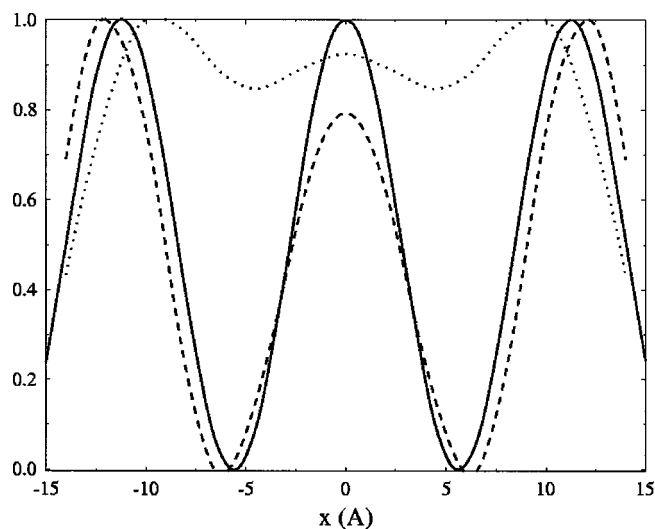

FIG. 5. Full line—the probability density, $\int dy \int dz |\psi(x,y,z)|^2$ (Å^{-1}), associated with the second excited cavity state normalized in the cavity $\times 0.0592$. Dashed line—$\bar{G}$ (see text; $nA \cdot V^{-1} \times 0.232$). Dotted lines, $I(\Phi = 742 \, \text{mV})$ ($nA \times 0.228$). The numerical constants are used to scale the maximum of each function to unity.
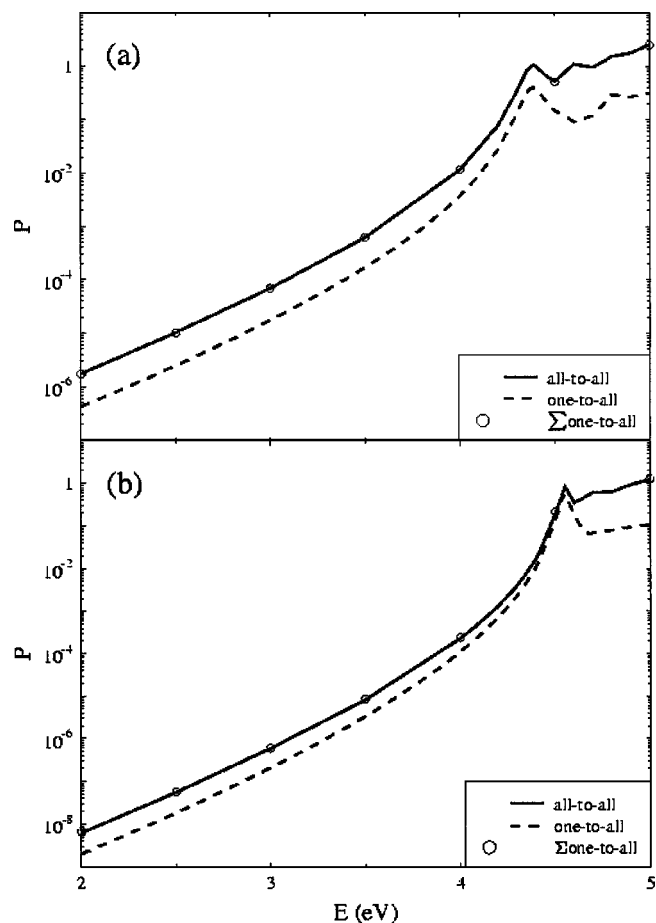

FIG. 6. One-to-all (dashed curves) and all-to-all (full curves) transmission probabilities of electron between two planar electrodes separated by (a) three and (b) four monolayers of water (see text for details). The circles sitting on the full lines are all-to-all transmission probabilities computed by summing the one-to-all probabilities over all incident directions relevant to the grid used.

B. Calculation of the cumulative tunneling flux in water

Another example of a calculation done in this way is shown in Figs. 6(a) and 6(b). These figures use configurations of water layers that were obtained from equilibrium trajectories of water (density 1 g/cm^3 and temperature 300 K) between two platinum (1,0,0) surfaces (see Refs. 8, 12 for details of the water, water-Pt, and water-electron potentials used). The electron-water pseudopotential is superimposed on a rectangular potential of height 5eV that represents the vacuum barrier. Figures 6(a) and 6(b) show the one-two-all (dashed lines) and the cumulative (all-to-all, full lines) transmission probabilities for particular configurations of water layers consisting of 3 and 4 monolayers, respectively. The cumulative transmission probabilities were obtained from Eq. (3) using self-energies calculated as described in Sec. III. The circle marks that practically sit on the full lines denote results of all-to-all transmission obtained by summing one-to-all transmission probabilities over all incident directions consistent with the grid used. The one-to-all probabilities were calculated from Eq. (8) as described in Ref. 8. In that work we discussed the existence of tunneling resonances in the range of ~ 1 eV below the vacuum barrier and their pos-

sible role in enhancing electron tunneling through water. We see that the cumulative transmission probabilities show the same resonance behavior. We note in passing that the cumulative quantities are sums over probabilities that can in principles exceed unity; in fact in the absence of a barrier where the transmission probability is 1 for all incident waves, the cumulative ''probability'' corresponds to the number of transversal channels. A full account of tunneling calculation in water is given elsewhere.[12,35]

V. CONCLUSION

This paper has described the numerical techniques used by us in recent works that calculate single electron transmission probabilities and the associated current in molecular junctions. We have focused on examples where the potential experienced by the electron is given as a local function of position, however similar formulations for other representations are easily derived. The calculation is based on evaluating electrostatic contributions to the electron-junction potential by numerically solving the relevant Laplace and Poisson equations, and by numerically evaluating tunneling probabilities by using iterative matrix inversion techniques to compute relevant elements of the electron Green's function, given proper care to self-energy terms that account for needed absorbing boundary conditions. Together, these techniques combine to yield an efficient numerical package to evaluate single electron transmission probabilities and current in molecular junctions of arbitrary geometries. Some simple applications demonstrate the power of this computational approach. More detailed applications in more realistic contexts are described elsewhere.

APPENDIX A: SELF-ENERGY CALCULATION

Here we briefly outline the procedure we use to calculate the self-energy matrices, $\mathbf{\Sigma}_L$ and $\mathbf{\Sigma}_R$, Eq. (20). This procedure is based on the renormalization-group technique of Refs. 24–26. This is a technique to evaluate both the bulk and the surface Green's function of a semi-infinite lattice with tight-binding coupling structure. We start by going to k-space in the directions x,y normal to the tunneling direction. Considering for example the right reservoir, it can, in this representation be written as a block matrix of the form

$$\mathbf{H}_R = \begin{bmatrix} \mathbf{H_{00}} & \mathbf{H_{01}} & 0 & 0 & 0 & \cdots \\ \mathbf{H_{01}^\dagger} & \mathbf{H_{00}} & \mathbf{H_{01}} & 0 & 0 & \cdots \\ 0 & \mathbf{H_{01}^\dagger} & \mathbf{H_{00}} & \mathbf{H_{01}} & 0 & \cdots \\ 0 & 0 & \mathbf{H_{01}^\dagger} & \mathbf{H_{00}} & \mathbf{H_{01}} & \cdots \\ \vdots & \vdots & \vdots & \vdots & \vdots & \ddots \end{bmatrix}, \quad (A1)$$

where the quadratic matrices $\mathbf{H_{00}}$ and $\mathbf{H_{01}}$ are of order n. n corresponds to the ''interaction range'' defined by the type of

finite difference approximation (FDA) scheme used for the kinetic energy operator, ($n=1$, 2 and 3 for the 3, 5 and 7-point FDA, respectively). The Green's function is defined by $(E-\mathbf{H}_R)\mathbf{G}_R=\mathbf{I}$ and its block elements are denoted below by $\mathbf{G}_{i,j}^{(R)}$. Explicit equations for these elements are

$$(E-\mathbf{H_{00}})\mathbf{G}_{00}^{(R)}=\mathbf{I}+\mathbf{H_{01}}\mathbf{G}_{10}^{(R)},$$

$$(E-\mathbf{H_{00}})\mathbf{G}_{10}^{(R)}=\mathbf{H_{01}^\dagger}\mathbf{G}_{00}^{(R)}+\mathbf{H_{01}}\mathbf{G}_{20}^{(R)},$$

...

$$(E-\mathbf{H_{00}})\mathbf{G}_{2n,0}^{(R)}=\mathbf{H_{01}^\dagger}\mathbf{G}_{2n-1,0}^{(R)}+\mathbf{H_{01}}\mathbf{G}_{2n+1,0}^{(R)},$$

$$(E-\mathbf{H_{00}})\mathbf{G}_{2n+1,0}^{(R)}=\mathbf{H_{01}^\dagger}\mathbf{G}_{2n,0}^{(R)}+\mathbf{H_{01}}\mathbf{G}_{2n+2,0}^{(R)}, \quad (A2)$$

...

$$(E-\mathbf{H_{00}})\mathbf{G}_{2n,2n}^{(R)}=\mathbf{I}+\mathbf{H_{01}^\dagger}\mathbf{G}_{2n-1,2n}^{(R)}+\mathbf{H_{01}}\mathbf{G}_{2n+1,2n}^{(R)},$$

$$(E-\mathbf{H_{00}})\mathbf{G}_{2n+1,2n}^{(R)}=\mathbf{H_{01}^\dagger}\mathbf{G}_{2n,2n}^{(R)}+\mathbf{H_{01}}\mathbf{G}_{2n+2,2n}^{(R)}.$$

...

Of particular interest are $\mathbf{G}_{00}^{(R)}$, the surface Green's function and $\mathbf{G}_{nn}^{(R)}$ ($n\to\infty$), the bulk Green's function. They will also be denoted below $\mathbf{G}_R^s$ (or $\mathbf{G}_L^s$ for the left reservoir) and $\mathbf{G}_B$. Next, the formal solutions for all elements with odd first index, i.e., elements of the type $\mathbf{G}_{2i+1,j}^{(R)}$, are inserted in the equations for elements with even first index, i.e., elements of the type $\mathbf{G}_{2i,j}^{(R)}$, to get

$$\begin{cases} (E-\mathcal{E}_1^s)\mathbf{G}_{0,0}^{(R)}=\mathbf{I}+\mathbf{A_1}\mathbf{G}_{2,0}^{(R)} \\ \cdots \\ (E-\mathcal{E}_1)\mathbf{G}_{2n,0}^{(R)}=\mathbf{B_1}\mathbf{G}_{2(n-1),0}^{(R)}+\mathbf{A_1}\mathbf{G}_{2(n+1),0}^{(R)} \\ \cdots \\ (E-\mathcal{E}_1)\mathbf{G}_{2n,2n}^{(R)}=\mathbf{I}+\mathbf{B_1}\mathbf{G}_{2(n-1),2n}^{(R)}+\mathbf{A_1}\mathbf{G}_{2(n+1),2n}^{(R)} \\ \cdots, \end{cases} \quad (A3)$$

with

$$\mathbf{A_1}=\mathbf{H_{01}}(E-\mathbf{H_{00}})^{-1}\mathbf{H_{01}},$$

$$\mathbf{B_1}=\mathbf{H_{01}^\dagger}(E-\mathbf{H_{00}})^{-1}\mathbf{H_{01}^\dagger},$$

$$\mathcal{E}_1^s=\mathbf{H_{00}}+\mathbf{H_{01}}(E-\mathbf{H_{00}})^{-1}\mathbf{H_{01}^\dagger}, \quad (A4)$$

$$\mathcal{E}_1=\mathbf{H_{00}}+\mathbf{H_{01}}(E-\mathbf{H_{00}})^{-1}\mathbf{H_{01}^\dagger}+\mathbf{H_{01}^\dagger}(E-\mathbf{H_{00}})^{-1}\mathbf{H_{01}}.$$

Equations (A4) define the first iteration ($i=1$) of an effective Hamiltonian

$$\mathbf{H}_R^{(i)}=\begin{bmatrix} \mathcal{E}_i^s & \mathbf{A}_i & 0 & 0 & 0 & \cdots \\ \mathbf{B}_i & \mathcal{E}_i & \mathbf{A}_i & 0 & 0 & \cdots \\ 0 & \mathbf{B}_i & \mathcal{E}_i & \mathbf{A}_i & 0 & \cdots \\ 0 & 0 & \mathbf{B}_i & \mathcal{E}_i & \mathbf{A}_i & \cdots \\ \vdots & \vdots & \vdots & \vdots & \vdots & \ddots \end{bmatrix} \quad (A5)$$

that for $i=1$ describes a chain of effective layers with a lattice constant $2a$, twice the original one. Renumbering indices in Eq. (A3) such that $2n\to n$ this procedure is continued to yield the iterative sequence

$$\mathbf{A}_i = \mathbf{A}_{i-1}(E - \mathcal{E}_{i-1})^{-1}\mathbf{A}_{i-1},$$

$$\mathbf{B}_i = \mathbf{B}_{i-1}(E - \mathcal{E}_{i-1})^{-1}\mathbf{B}_{i-1},$$

$$\mathcal{E}_i^s = \mathcal{E}_{i-1}^s + \mathbf{A}_{i-1}(E - \mathcal{E}_{i-1})^{-1}\mathbf{B}_{i-1}, \tag{A6}$$

$$\mathcal{E}_i = \mathcal{E}_{i-1} + \mathbf{A}_{i-1}(E - \mathcal{E}_{i-1})^{-1}\mathbf{B}_{i-1}$$
$$+ \mathbf{B}_{i-1}(E - \mathcal{E}_{i-1})^{-1}\mathbf{A}_{i-1},$$

starting with $\mathcal{E}_0^s = \mathcal{E}_0 = \mathbf{H}_{00}$, $\mathbf{A}_0 = \mathbf{H}_{01}$, and $\mathbf{B}_0 = \mathbf{H}_{01}^\dagger$. Equations (A5) and (A6) define an effective Hamiltonian for a chain of lattice constant $2^i a$. Iterations are repeated until the renormalized nearest neighbor interactions $\mathbf{A}_i$ and $\mathbf{B}_i$ are small enough to be disregarded. At this stage the surface Green's functions of the right reservoir may be written as

$$\mathbf{G}_R^s(E) \approx (E - \mathcal{E}_i^s)^{-1}. \tag{A7}$$

This is the Green's function needed in Eqs. (23)–(24). The bulk Green's function can also be identified as $\mathbf{G}_B(E) \approx (E - \mathcal{E}_i)^{-1}$. The Green function for the left contact is given by

$$\mathbf{G}_L^s(E) \approx (E - \widetilde{\mathcal{E}}_i^s)^{-1}, \tag{A8}$$

where $\widetilde{\mathcal{E}}_i^s$ is obtained by iterating

$$\widetilde{\mathcal{E}}_i^s = \widetilde{\mathcal{E}}_{i-1}^s + \mathbf{B}_{i-1}(E - \mathcal{E}_{i-1})^{-1}\mathbf{A}_{i-1} \tag{A9}$$

starting with $\widetilde{\mathcal{E}}_0^s = \mathbf{H}_{00}$, until $\widetilde{\mathcal{E}}_i^s \approx \widetilde{\mathcal{E}}_{i-1}^s$.

APPENDIX B: THE CASE OF NONORTHOGONAL BASIS

While not encountered in the present paper, the need to use the Green's function techniques described in Sec. III and Appendix A often arises when using overlapping basis functions. For completeness we describe here the procedure that should replace Appendix A in such cases.

When using a basis with overlap, the system partition is not as straightforward as it is for the orthogonal basis sets. In particular, partitioning of the Schrödinger equation and partitioning of the Green function equation are not equivalent.[36,37] The latter, which is relevant for the purpose of describing subsystem dynamics, cannot be implemented rigorously for the infinite subspace representing the lead. A useful approximation is obtained by expanding in the overlap between the subspace and the rest of the overall system.[37] To the lowest order this yields the result identical to that obtained from partitioning the Schrödinger equation

$$\Sigma_K(E) = (E\mathbf{S}_{MK} - \mathbf{H}_{MK})\mathcal{G}_K(E)(E\mathbf{S}_{KM} - \mathbf{H}_{KM}), \tag{B1}$$

where

$$\mathcal{G}_K(E) = [E\mathbf{S}_{KK} - \mathbf{H}_{KK}]^{-1}. \tag{B2}$$

Note that $\mathcal{G}_K(E)$ is not the Green function of the system $\mathbf{K}$. The Green function in a nonorthogonal basis is obtained from

$$\mathbf{G}(E) = \mathbf{S}[E\mathbf{S} - \mathbf{H}]^{-1}\mathbf{S}. \tag{B3}$$

Here we generalize the renormalization-group technique outlined in Appendix A for the case of nonorthogonal bases and show the algorithm for calculating $\mathcal{G}(E)$ as well-as surface and bulk Green functions $\mathbf{G}(E)$ of the leads.

Consider the lead Hamiltonian (A1) and the corresponding matrix $\mathcal{G}$

$$\mathcal{G}_R(E) = \mathbf{S}_R^{-1}\mathbf{G}_R\mathbf{S}_R^{-1} = [E\mathbf{S}_R - \mathbf{H}_R]^{-1}. \tag{B4}$$

Equation (B3) for the lead Green function, $(E\mathbf{S}_R - \mathbf{H}_R)\mathbf{S}_R^{-1}\mathbf{G}_R = \mathbf{S}_R$ can be rewritten in terms of $\mathcal{G}_R$ as

$$(E\mathbf{S}_R - \mathbf{H}_R)\mathcal{G}_R = \mathbf{I}. \tag{B5}$$

Proceeding as in the case of orthogonal basis (Appendix A), i.e., writing equations for the different blocks of the Hamiltonian and overlap matrices and using substitution to sequentially exclude equations with odd indices, one gets a modified version of the iterative procedure (A6)

$$\mathbf{A}_i = \mathbf{A}_{i-1}(E\mathbf{S}_{00} - \mathbf{H}_{00})^{-1}\mathbf{A}_{i-1},$$

$$\mathbf{B}_i = \mathbf{B}_{i-1}(E\mathbf{S}_{00} - \mathbf{H}_{00})^{-1}\mathbf{B}_{i-1},$$

$$\mathcal{E}_i^s = \mathcal{E}_{i-1}^s + \mathbf{A}_{i-1}(E\mathbf{S}_{00} - \mathbf{H}_{00})^{-1}\mathbf{B}_{i-1}, \tag{B6}$$

$$\widetilde{\mathcal{E}}_i^s = \widetilde{\mathcal{E}}_{i-1}^s + \mathbf{B}_{i-1}(E\mathbf{S}_{00} - \mathbf{H}_{00})^{-1}\mathbf{A}_{i-1},$$

$$\mathcal{E}_i = \mathcal{E}_{i-1} + \mathbf{A}_{i-1}(E\mathbf{S}_{00} - \mathbf{H}_{00})^{-1}\mathbf{B}_{i-1}$$
$$+ \mathbf{B}_{i-1}(E\mathbf{S}_{00} - \mathbf{H}_{00})^{-1}\mathbf{A}_{i-1},$$

with the starting values $\mathbf{A}_0 = -\mathbf{h}_{00}$, $\mathbf{B}_0 = -\mathbf{h}_{01}^\dagger$, $\mathcal{E}_0^s = \widetilde{\mathcal{E}}_0^s = \mathbf{H}_{00}$, where $\mathbf{h}_{ij} \equiv E\mathbf{S}_{ij} - \mathbf{H}_{ij}$.

After convergence, i.e., when $\mathcal{E}_i \approx \mathcal{E}_{i-1}$ (and similarly for $\mathcal{E}_i^s$ and $\widetilde{\mathcal{E}}_i^s$) to the desired accuracy, the surface and bulk blocks of the matrix $\mathcal{G}$ are given by

$$\mathcal{G}_L^s(E) = (E\mathbf{S}_{00} - \mathcal{E}_i^s)^{-1},$$

$$\mathcal{G}_R^s(E) = (E\mathbf{S}_{00} - \widetilde{\mathcal{E}}_i^s)^{-1}, \tag{B7}$$

$$\mathcal{G}_B(E) = (E\mathbf{S}_{00} - \mathcal{E}_i)^{-1}.$$

This is in fact all we need to evaluate the approximation (B1) for the self-energy. The actual Green functions may also be obtained. It is straightforward to show that

$$\mathbf{G}_R(E) = \mathbf{G}_{00}^{(R)} = \mathbf{S}_{00}\mathcal{G}_{00}^{(R)}\mathbf{S}_{00} + \mathbf{S}_{01}\mathcal{G}_{10}^{(R)}\mathbf{S}_{00} + \mathbf{S}_{00}\mathcal{G}_{01}^{(R)}\mathbf{S}_{01}^\dagger$$
$$+ \mathbf{S}_{01}\mathcal{G}_{11}^{(R)}\mathbf{S}_{01}^\dagger, \tag{B8}$$

$$\mathbf{G}_L(E) = \mathbf{G}_{00}^{(L)} = \mathbf{S}_{00}\mathcal{G}_{00}^{(L)}\mathbf{S}_{00} + \mathbf{S}_{01}^\dagger\mathcal{G}_{10}^{(L)}\mathbf{S}_{00} + \mathbf{S}_{00}\mathcal{G}_{01}^{(L)}\mathbf{S}_{01}$$
$$+ \mathbf{S}_{01}^\dagger\mathcal{G}_{11}^{(L)}\mathbf{S}_{01}, \tag{B9}$$

$$\mathbf{G}_B(E) = \mathbf{G}_{nn}^{(B)} = \mathbf{S}_{01}^\dagger\mathcal{G}_{n-1,n-1}^{(B)}\mathbf{S}_{01} + \mathbf{S}_{00}\mathcal{G}_{n,n-1}^{(B)}\mathbf{S}_{01}$$
$$+ \mathbf{S}_{01}\mathcal{G}_{n+1,n-1}^{(B)}\mathbf{S}_{01} + \mathbf{S}_{01}^\dagger\mathcal{G}_{n-1,n}^{(B)}\mathbf{S}_{00}$$
$$+ \mathbf{S}_{00}\mathcal{G}_{n,n}^{(B)}\mathbf{S}_{00} + \mathbf{S}_{01}\mathcal{G}_{n+1,n}^{(B)}\mathbf{S}_{00}$$
$$+ \mathbf{S}_{01}^\dagger\mathcal{G}_{n-1,n+1}^{(B)}\mathbf{S}_{01}^\dagger + \mathbf{S}_{00}\mathcal{G}_{n,n+1}^{(B)}\mathbf{S}_{01}^\dagger$$
$$+ \mathbf{S}_{01}\mathcal{G}_{n+1,n+1}^{(B)}\mathbf{S}_{01}^\dagger, \tag{B10}$$

where $\mathcal{G}_{00}^{(R)} = \mathcal{G}_R$, $\mathcal{G}_{00}^{(L)} = \mathcal{G}_L$, and where $\mathcal{G}_{n,n}^{(B)} = \mathcal{G}_{n-1,n-1}^{(B)} = \mathcal{G}_{n+1,n+1}^{(B)} = \mathcal{G}_B$. After some algebra one gets expressions also for the other matrix elements in Eqs. (B8)–(B10)

$$\mathcal{G}_{11}^{(R)} = (E\mathbf{S}_{00} - \mathcal{E}_i^p)^{-1},$$

$$\mathcal{G}_{10}^{(R)} = \mathbf{h}_{01}^{-1}(\mathbf{I} - \mathbf{h}_{00}\mathcal{G}_{00}^{(R)}),$$

$$\mathcal{G}_{01}^{(R)} = -\mathbf{h}_{00}^{-1}\mathbf{h}_{01}\mathcal{G}_{11}^{(R)},$$

$$\mathcal{G}_{11}^{(L)} = (E\mathbf{S}_{00} - \widetilde{\mathcal{E}}_i^p)^{-1},$$

$$\mathcal{G}_{10}^{(L)} = [\mathbf{h}_{01}^\dagger]^{-1}(\mathbf{I} - \mathbf{h}_{00}\mathcal{G}_{00}^{(L)}),$$

$$\mathcal{G}_{01}^{(L)} = -\mathbf{h}_{00}^{-1}\mathbf{h}_{01}^\dagger\mathcal{G}_{11}^{(L)},$$ (B11)

$$\mathcal{G}_{n,n-1}^{(B)} = \mathcal{G}_{n+1,n}^{(B)} = -(E\mathbf{S}_{00} - \mathcal{E}_i^s)^{-1}\mathbf{h}_{01}^\dagger\mathcal{G}_{n,n}^{(B)},$$

$$\mathcal{G}_{n-1,n}^{(B)} = \mathcal{G}_{n,n+1}^{(B)} = -(E\mathbf{S}_{00} - \widetilde{\mathcal{E}}_i^s)^{-1}\mathbf{h}_{01}\mathcal{G}_{n,n}^{(B)},$$

$$\mathcal{G}_{n+1,n-1}^{(B)} = (E\mathbf{S}_{00} - \mathcal{E}_i^p)^{-1}\mathbf{h}_{01}^\dagger\mathbf{h}_{00}^{-1}\mathbf{h}_{01}^\dagger\mathcal{G}_{n,n}^{(B)},$$

$$\mathcal{G}_{n-1,n+1}^{(B)} = (E\mathbf{S}_{00} - \widetilde{\mathcal{E}}_i^p)^{-1}\mathbf{h}_{01}\mathbf{h}_{00}^{-1}\mathbf{h}_{01}\mathcal{G}_{n,n}^{(B)},$$

where

$$\mathcal{E}_i^p = \mathcal{E}_i^s + \mathbf{h}_{01}^\dagger\mathbf{h}_{00}^{-1}\mathbf{h}_{01},$$

$$\widetilde{\mathcal{E}}_i^p = \widetilde{\mathcal{E}}_i^s + \mathbf{h}_{01}\mathbf{h}_{00}^{-1}\mathbf{h}_{01}^\dagger,$$ (B12)

$$\mathbf{h}_{00} = E\mathbf{S}_{00} - \mathbf{H}_{00}.$$

Equations (B8)–(B12) provide the route for calculating the Green's function, if needed.

[1] R. A. Marcus, J. Chem. Phys. **24**, 966 (1956).

[2] R. A. Marcus, J. Chem. Phys. **24**, 979 (1956).

[3] A. Nitzan, Annu. Rev. Phys. Chem. **52**, 681 (2001).

[4] In our applications we have used the equivalent 7 point differencing approximation $\partial^2/\partial x^2 \Phi_{i,j,k} = h_x^{-2}[\Phi_{i+3,j,k}/90 - 3\Phi_{i+2,j,k}/20 + 3\Phi_{i+1,j,k}/2 - 49\Phi_{i,j,k}/18 + 3\Phi_{i-1,j,k}/2 - 3\Phi_{i-2,j,k}/20 + \Phi_{i-3,j,k}/90]$.

[5] Equation (3) holds provided there is no direct coupling between the electrodes. In the local representation used in this paper this is practically always true.

[6] See, e.g., S. Datta, *Electric Transport in Mesoscopic Systems* (Cambridge University Press, Cambridge, 1995).

[7] D. Evans, I. Benjamin, T. Seideman, H. T. Ezer, and A. Nitzan, Abstr. Pap. - Am. Chem. Soc. **212**, 194-COLL (1996).

[8] U. Peskin, A. Edlund, I. Bar-On, M. Galperin, and A. Nitzan, J. Chem. Phys. **111**, 7558 (1999).

[9] M. Galperin, A. Nitzan, and U. Peskin, J. Chem. Phys. **114**, 9205 (2001).

[10] I. Benjamin, D. Evans, and A. Nitzan, J. Chem. Phys. **106**, 1291 (1997).

[11] I. Benjamin, D. Evans, and A. Nitzan, J. Chem. Phys. **106**, 6647 (1997).

[12] A. Nitzan and I. Benjamin, Acc. Chem. Res. **32**, 854 (1999).

[13] A. Mosyak, P. Graf, I. Benjamin, and A. Nitzan, J. Phys. Chem. A **101**, 429 (1997).

[14] J. G. Simmons, J. Appl. Phys. **34**, 1793 (1963).

[15] Y. Saad, *Iterative Methods for Sparse Linear Systems* (PWS Publishing, Boston, 1996).

[16] S. Balay, W. D. Gropp, L. C. McInnes, and B. F. Smith (2000).

[17] P. Graf, A. Nitzan, M. G. Kurnikova, and R. D. Coalson, J. Phys. Chem. B **104**, 12324 (2000).

[18] W. H. Press, S. A. Teukolsky, W. T. Vetterling, and B. P. P. Flannery, *Numerical Recipes: The Art of Scientific Computing*, 2nd ed. (Cambridge University Press, London, 1992).

[19] On the grid this contribution is not singular, but is still unphysical and has to be subtracted.

[20] V. Y. Arsenin, *Basic Equations and Special Functions of Mathematical Physics* (Iliffe Book, London, 1968).

[21] K. S. Dy, S.-Y. Wu, and T. Spratlin, Phys. Rev. B **20**, 4237 (1979).

[22] S. Y. Wu, Z. L. Xie, and N. Potoczak, Phys. Rev. B **48**, 14826 (1993).

[23] S. Y. Wu, J. Cocks, and C. S. Jayanthi, Phys. Rev. B **49**, 7957 (1994).

[24] F. Guinea, T. Tejedor, F. Flores, and E. Louis, Phys. Rev. B **28**, 4397 (1983).

[25] M. P. Lopez-Sancho, L. M. Lopez-Sancho, and J. Rubio, J. Phys. F: Met. Phys. **14**, 1205 (1984).

[26] M. P. Lopez-Sancho, L. M. Lopez-Sancho, and J. Rubio, J. Phys. F: Met. Phys. **15**, 851 (1985).

[27] A. Umerski, Phys. Rev. B **55**, 5266 (1997).

[28] N. Moiseyev, J. Phys. B **31**, 1431 (1998).

[29] R. Zavin, I. Vorobeichik, and N. Moiseyev, Chem. Phys. Lett. **288**, 413 (1998).

[30] Equation (21) expresses the fact that removing the surface S from the semi-infinite reservoir R leaves a system identical to the original R.

[31] S. N. Yaliraki, M. Kemp, and M. A. Ratner, J. Am. Chem. Soc. **121**, 3428 (1999).

[32] L. C. Venema, J. W. G. Wildoer, J. W. Janssen, S. J. Tans, H. L. J. T. Tuinstra, L. P. Kouwenhoven, and C. Dekker, Science **283**, 52 (1999).

[33] The choice of relatively small values for the barrier height and the work function saves numerical work by making it possible to use in this numerical example a relatively coarse grid.

[34] Obviously a better result would be obtained by taking a smaller Φ interval that contains the desired resonance state, i.e. by taking the numerical derivative $dI/d\Phi$ at resonance. Note that using the Landauer formula for the conduction instead of numerically evaluating this derivative is valid only in the linear conduction regime. In the general case it misses the dependence of the transmission probability on the voltage.

[35] M. Galperin, A. Nitzan, and I. Benjamin, J. Phys. Chem. (in press).

[36] I. V. Kurnikov and D. N. Beratan, J. Chem. Phys. **105**, 9561 (1996).

[37] S. Priyadarshy, S. S. Skourtis, S. M. Risser, and D. N. Beratan, J. Chem. Phys. **104**, 9473 (1996).